

Received 1 May 2024, accepted 17 May 2024, date of publication 23 May 2024, date of current version 3 June 2024.

Digital Object Identifier 10.1109/ACCESS.2024.3404635

APPLIED RESEARCH

3D Surface Reconstruction of Car Body Based on Any Single View

BO WANG¹, QI WU¹, HUAWEI WANG¹, LI HU¹, AND BAOJUN LI², (Member, IEEE)

¹School of Automobile and Traffic Engineering, Wuhan University of Science and Technology, Wuhan 430065, China

²School of Automotive Engineering, Dalian University of Technology, Dalian 116024, China

Corresponding author: BaoJun Li (bjli@dlut.edu.cn)

This work was supported by the National Natural Science Foundation of China under Grant 52375260 and Grant 51905389.


ABSTRACT With the continuous development of the automobile industry, fast and efficient body styling methods have become crucial. Although traditional hand-drawn sketches and 3D modeling are feasible, they often consume lots of time, manpower and financial resources when faced with complex design requirements. Therefore, a quick method for car body modeling has become a hot topic in automotive design. This paper proposes a three-dimensional automotive wireframe model generation and surface reconstruction method based on a single image in any view. Firstly, 3D wireframe model generation for a single car image in any view. By the MobileNet V2 network trained based on the established 2D car body library USMV3085, the visual angle of a specific single car image in any view can be identified, following the relevant wireframe model can be generated with the weight coefficients computed by constrained least squares method according to the key points and the corresponding rotated key points of the 3D wireframe library. Secondly, the corresponding 3D surface is reconstructed automatically. With the skeleton line firstly computed by the Skeleton Generation Algorithm for every 2D projected split part of the 3D wireframe model, corresponding 3D boundary relation pairs and control polygons are obtained, following the 3D surface is reconstructed integrating all split parts. Compared to traditional computer-aided shape design, this automatic method greatly shortens the research and development cycle and has certain reference significance in car body design.

INDEX TERMS Single view body modeling, skeleton line extraction, surface reconstruction.

I. INTRODUCTION

In the field of automobile design, body design is an important part [1]. In the conceptual design phase, designers create 3D body models by hand-drawing 2D sketches from various perspectives using 3D modeling software. Popular 3D modeling software includes Catia [2] and Solidworks [3]. But complex body designs can lead to lots of 3D modeling work that consumes additional human, time, and money resources. How to quickly model the car body through the single view of the car, so as to shorten the development cycle, is a very valuable research field.

The main process is as follows: 1) Establish and expand the automobile 3D wireframe model library (Fig.1(b)); 2) Select some key points of the 2D car body image in any view (Fig.1(d)) and discriminate the visual angle by the MobileNet

The associate editor coordinating the review of this manuscript and approving it for publication was Orazio Gambino .

V2 network based on the USMV3085 (Fig.1(c)); 3) According to the visual angle and the model library, the weight coefficients can be computed by constrained least squares method for the corresponding models; 4) Divide the car surface into some blocks according to the body parts (Fig.1(f)), and generate the Skeleton line for every block by the Skeleton Generation Algorithm for Complex Shape (Fig.1(h)), further the 3D control meshes (Fig.1(i)) and the surface (Fig.1(j)) for the complex 3D shape; 5) Integrate all complex surfaces to achieve the reconstruction of the three-dimensional surface of the car body (Fig.1(k)). The complete workflow of the wireframe model and surface reconstruction is shown in Fig.1.

II. RELATED WORKS

A. THREE-DIMENSIONAL RECONSTRUCTION

3D reconstruction refers to the process of generating corresponding 3D objects or scenes from given 2D images or

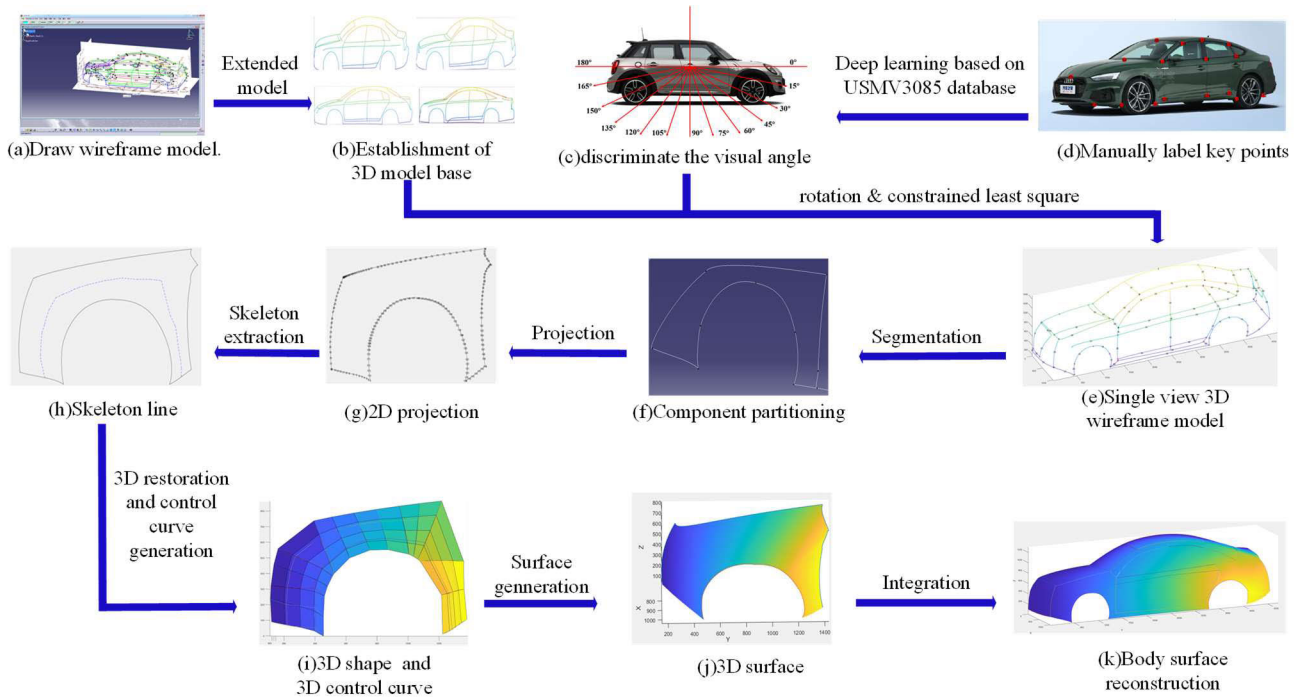


FIGURE 1. Model reconstruction flow.

other forms of data through calculation and inference. Common 3D reconstruction methods include stereovision [5], stereomatching [6], point cloud reconstruction [7], and voxel reconstruction [8]. Liu et al. [9] proposed a new framework called PlaneMVS for 3D plane reconstruction from multiple input views with known camera poses. Liu et al. [10] proposed a practical 3D reality reconstruction framework Deep3D, which was paired with a Multi-view stereo (MVS) matching model based on deep learning and Adaptive Multi-view Aggregate matching (Ada-MVS) model to obtain a 3D texture grid model from multi-view oblique aerial images. Chen and Zuo [11] proposed a two-stage training network 3D-ARNet based on the reconstruction of point clouds from a single image. Hou et al. [12] proposed a high-quality voxel 3D reconstruction system for large scenes based on branch and binding methods, which can reliably find the best attitude data and has a high-precision dense 3D model. Based on the idea of 3D reconstruction, this paper combines image information and mathematical algorithms to reconstruct the automobile surface automatically. In areas without sufficient texture, such as monochrome backgrounds or clear glass surfaces, stereo vision methods may not be able to match corresponding points, resulting in low reconstruction accuracy effectively; In areas with discontinuous textures or object edges, stereo matching may produce discontinuous parallax problems, resulting in noise or discontinuous areas in the depth image; Point cloud reconstruction and voxel reconstruction have high reconstruction accuracy, but the computational complexity is very high and require a lot of computing resources and time. In response to the problems

of the above methods, this paper, based on the idea of 3D reconstruction, combines image information and mathematical algorithms to automatically reconstruct the car surface.

B. SINGLE-VIEW BODY MODELING

Single-view 3D reconstruction refers to the reconstruction and recovery of 3D objects using a single image. This field combines the knowledge of many fields, such as computer vision, image processing, computer graphics, etc., and has received extensive attention and research in recent years. Common 3D reconstruction methods are divided into feature point based [13] and deep learning based [14]. Han et al. [15] proposed a 3D reconstruction method based on image feature point matching. By improving SIFT, the initial matching of feature points is achieved by using the neighborhood voting method, and then the initial matching points are optimized by using the improved RANSAC algorithm, and a new SFM reconstruction method is obtained. Engelmann et al. [16] proposed a key point detector that positions an object as a central point and predicts all object attributes directly, i.e. it selects an example shape from a given database. Fu et al. [17] uses a data-driven deep learning framework to automatically detect and classify building elements from the laser-scanned point cloud scene, and uses a point-based object classifier to determine the type of building component according to the segmentation point, and matches each detected object with the corresponding BIM entity according to the nearest neighbor in the feature space. This paper takes the 3D wireframe reconstruction of the automobile as an example, by establishing the 3D wireframe model library of

automobiles and determining the key points of a single view using the MobileNet V2 deep learning network.

C. SKELETON LINE EXTRACTION

Skeleton line extraction refers to the extraction of skeleton lines or central axes representing the main structure and shape of objects from images or three-dimensional models, to extract the skeleton outline of objects to carry out concise geometric and topological expression of objects, reduce the size of data, and facilitate shape analysis and processing of objects. At present, the commonly used skeleton line extraction methods include the grass fire transformation method [18], the Voronoi diagram method [19], and the maximum circle cutting method [20]. Duan et al. [21] proposed a new skeleton-based motion recognition method, called PoseConv-3D. Compared with GCN [22], PoseConv3D is more effective in learning spatiotemporal features and more robust in pose estimation noise. Hu et al. [23] proposed a new multi-scale time sampling module and depth spatiotemporal feature extraction module, which strengthened the receptive field of feature maps and enhanced the extraction of spatiotemporal-related feature information through the network. For objects with complex shapes, the grass-fire transformation method may produce broken or erroneous central axes. The Voronoi diagram is susceptible to noise and edge discontinuities, which may cause the generated skeleton line to be not smooth enough or broken. For objects with multiple connected parts or complex geometric shapes, the maximum circle method cutting may generate too many branches or unnecessary details, resulting in the extracted skeleton line being too complex. Based on the above problems, this paper proposes a new skeleton extraction method that can quickly realize skeleton extraction of complex wireframes.

D. SURFACE RECONSTRUCTION

Surface reconstruction can restore continuous 3D surface models from discrete data representations. This is important for processing and analyzing data obtained from the real world. Surface reconstruction is a diverse and challenging field that involves many different methods and techniques. Point cloud [24] is one of the common data representations in surface reconstruction, which can accurately capture aggregated information about an object's surface. Voxels [25] are discrete data representations in three-dimensional space. Surface reconstruction can generate a surface model by processing voxel data. Lv et al. [26] proposed a grid reconstruction framework based on a 3D point cloud structure. Preliminary reconstructed grids can be obtained according to the detected local regions. Through grid optimization, the initially reconstructed grids are optimized into isotropic grids with significant geometric features. Ummenhofer et al. [27] proposed generalized convolution kernel for 3D reconstruction using ConvNets of point clouds. This method uses a multi-scale convolution kernel and can be applied to adaptive

meshes generated using octree. Point cloud data usually comes from sensor acquisition or other methods, which may contain noise and incompleteness. This can directly affect the quality of the reconstruction results. The voxel reconstruction algorithm involves the setting of some parameters, such as voxel size, smoothing parameters, etc, but the parameter set needs to be adjusted empirically, and different parameter settings may lead to completely different reconstruction effects. To address the above problems, this paper uses the skeleton lines of the complex shapes of the detected body parts to automatically realize the surface reconstruction of the 3D wireframe model of the car.

E. ESTABLISHMENT OF AUTOMOBILE 3D WIRE-FRAME MODEL LIBRARY

NURBS [28] is widely used in automobile modeling for complex parts design, in which the shape is constrained by the control points. Bézier curves were developed by the French engineer Pierre Bézier in the 1960s for use in the field of automotive design. It is widely used in 2D and 3D graphics, such as drawing curves, creating fonts, modeling objects, and so on [29]. The special cubic Bézier curve is composed of 4 control points with C2 continuity to meet the requirements of car styling. The automobile 3D wire-frame model library is created by Catia software based on the front, back, side, and top views of the automobile design drawings. Each model is composed of 70 cubic Bézier curves. The specific steps are as follows: 1) Draw 70 standard cubic Bézier curve template manually, as shown in Fig.2 in matlab software; 2) Enter the sketch tracer interface in Catia, select the corresponding view mode, import the four views of the car in sequence, adjust the proportional size of the coordinate axes according to the actual size given on the car design drawing, and the final effect is shown in Fig.3(a); 3) Insert the standard curve template parts drawn in step 1), as shown in Fig.3(b); 4) For each three-dimensional curve, drag the control points in the four views to match the real position of the curve; 5) Export the curve model as *.stp file, which is used to generate all the data coordinates of the wireframe model. 6). Repeat the above steps to obtain 3D wireframe models of different types and models of automobiles, and finally establish a database composed of 14 hand-built wireframe models.

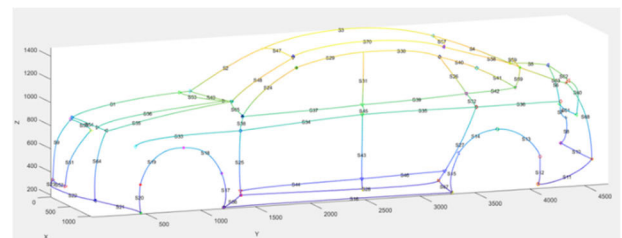


FIGURE 2. 3D wireframe model.

To normalize the model base constructed in this paper, all models were translated and scaled with the front wheel as the base point, and the wheel center of the calibrated

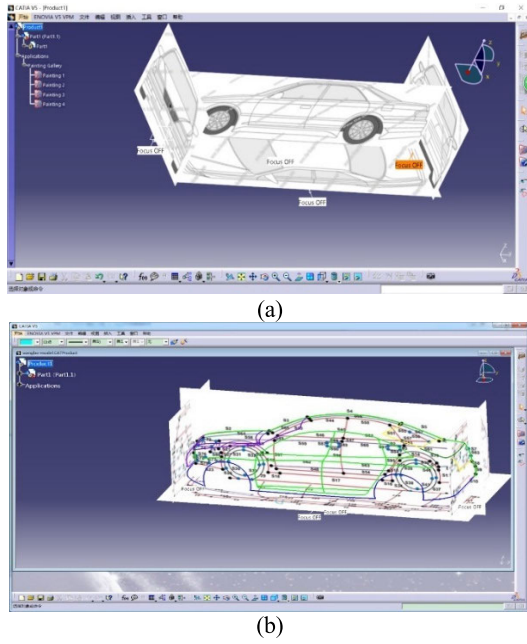


FIGURE 3. Effect after importing the four views and Effect after importing the standard curve template. (a) Import car four view.(b) Draw a wireframe model.

model was (0,0) for the front wheel and (1000,0) for the rear wheel. Define the shape of the model vector $s_i = (X_1^i, Y_1^i, Z_1^i, X_2^i, Y_2^i, Z_2^i, \dots, X_n^i, Y_n^i, Z_n^i)^T$, of which $i = 1 : 14, n = 70 \times 4 = 280$. The shape vectors of the 14 calibrated 3D models are denoted as s_i ; matrix $S = (s_1^T, s_2^T, \dots, s_{14}^T)^T$.

To further expand the wire-frame model library, the specific methods are as follows: 1) Firstly, zoom the height of every model. Scale key points whose Z-axis value is higher than the center point by multiplying 0.7, 0.8, 0.9, 1.1 and 1.2 respectively, and then incorporate them into the model library after scaling; 2) Secondly, Scale the key points whose Y-axis value is smaller than the back point of the front overhang (the intersection point of S20 and S21) by multiplying 0.8, 0.9 and 1.1 respectively, and scale the key points whose Y-axis value is greater than the Y-value of the front point of the rear overhang (the intersection point of S11 and S12) by the multiplying 0.8, 0.9 and 1.1 respectively, and then incorporate them into the model library after scaling; 3) The X-axis values of all key points are multiplied by 0.7, 0.8, 0.9, 1.1, and 1.2 respectively. Then incorporate them into the model database after scaling. After the above steps, the final number of 3D wire-frame models in the model library is 3528, with the expanded model library is $S = (s_1^T, s_2^T, s_3^T \dots s_{3528}^T)^T$.

III. SINGLE VIEW 3D WIREFRAME MODELING

A. ESTABLISHMENT OF DIFFERENT VIEW DATA SETS

Data sets such as front, side and rear views of the car can be easily collected from the Internet, and other views of the body from different angles can be generated by rendering software. In this paper, 150 automobile models were selected from the ShapeNet dataset, each model was rendered with

KeyShot 6.3 software, and the multi-angle automobile image database USMV3085 was established by itself. The angle classification is from 0° to 180°, with an interval of 15°, as shown in Fig.4. Tab.1 is an example of one car for the different angle categories and relative samples contained in USMV3085.

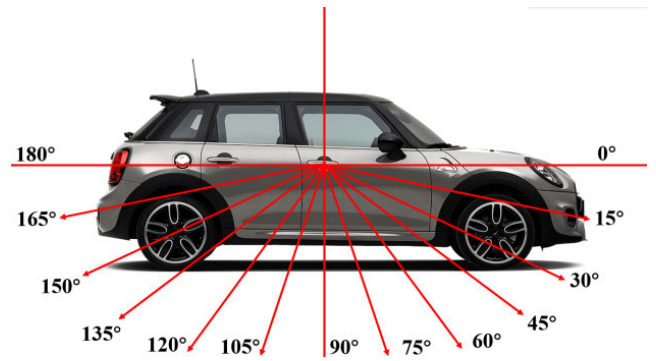


FIGURE 4. Angle acquisition standard.

TABLE 1. Data related to model library expansion.

Angle	0°	15°	30°
Sample			
Angle	45°	60°	75°
Sample			
Angle	90°	105°	120°
Sample			
Angle	135°	150°	165°
Sample			

TABLE 2. Different angle categories and relative examples contained in USMV3085.

Number of expansions	Extension Method	Initial number	Final number
1	Scaling along the Z-axis	14	84
2	Scaling along the Y-axis	84	588
3	Scaling along the X-axis	588	3528

B. SINGLE VIEW ANGLE ESTIMATION BASED ON IMPROVED MOBILENET V2

MobileNet network is a lightweight convolutional neural network suitable for mobile devices or embedded devices, compared with traditional convolutional neural networks,

the number of model parameters and the amount of computation are greatly reduced [30]. Compared with traditional convolutional neural networks. The core idea of MobileNet V1 is to use dept-separable convolution to replace standard convolution operations, but there are some problems: 1) Self-convolution cannot change the number of channels, if the channel number of the input is small, it can only be used for low-dimensional feature extraction, and the effect is not good; 2) The inability to reuse the features. MobileNet V2 can solve the above problems well [31].

Transfer learning refers to applying pre-trained model parameters to a new model to help the new model train, transfer annotated data or knowledge structure from related fields, and complete or improve the learning effect in the field of target recognition [32]. It can not only shorten the training cycle of the model but also improve the test accuracy and reduce the training loss rate. Therefore, in this paper, the Mo-bileNet V2 model is used to train the data set containing the automobile Angle label, and transfer learning is combined to complete the identification of the automobile angle.

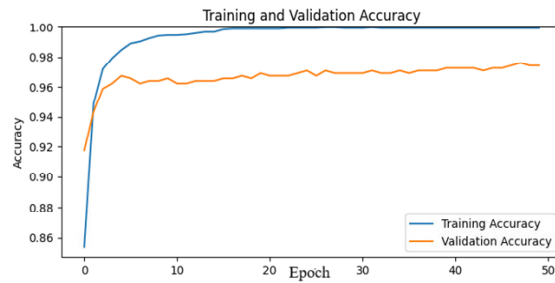
The processed data will be named with 13 filenames of 0°, 15°, 30°, 45°, 60°, 75°, 90°, 105°, 120°, 135°, 150°, 165°, 180°, as a label during training. After pre-processing the collected 3-085 multi-view image data, in order to facilitate the training and testing of the model in deep learning, the data set is randomly divided into the training set and the verification set according to the ratio of 8:2. The experimental operating system is Windows 10, and the CPU model is Intel Core i5-1126-0H@2.60 GHz. Through Python programming, MobileNet V2 was used to build the network model under the TensorFlow framework, and then training was carried out. The model parameters were set to Image Resize = 64×64, Learning Rate= 0.001, Epoch = 50, Batch Data = 64, and the trained model was saved as Car-MobileNet.

The recognition accuracy of the vehicle view Angle recognition system based on the MobileNetV2 network and created by the method of ab initio training is about 97% on the verification set, and the error analysis is shown in Fig.5.

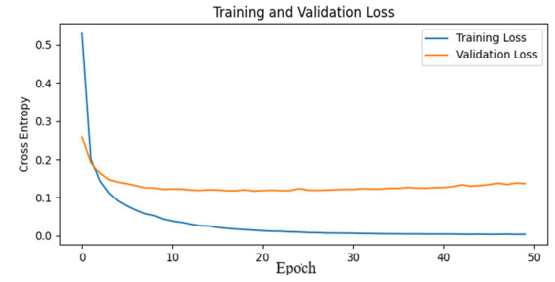
In this paper, the transfer learning method is used to build a vehicle view Angle recognition system with small data sets, which has a high recognition accuracy and can be used for the next step of fast model matching and reconstruction.

C. KEY POINTS IN A SPECIFIC SINGLE VIEW

The key points are related to the accuracy of the targeted reconstructed model. Too many key points will lead to bigger reconstruction error, while too few will lead to the loss of key information, resulting in too low accuracy of subsequent reconstruction [33]. At the same time, considering the point set matching with the template, this paper selects 35 key points {Key P_i|i = 1 : 35} on the three-dimensional template, as shown in Fig.6.



(a)



(b)

FIGURE 5. Error analysis of angle recognition for car images. (a) Training set and verification set accuracy.(b) Training set and verification set errors.

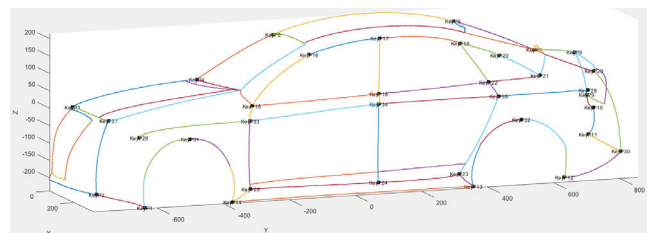


FIGURE 6. 35 key points for the 3D wireframe template.

D. 3D WIREFRAME RECONSTRUCTION

For automobile 3D wire-frame model database {S_i}_{i=1}^m, when m is large enough, all the models in the database can be used as the base and a new model can be obtained by linear combination of different weight coefficients. The model contribution coefficient vector H is defined, whose element H_i represents the contribution of the ith automobile model in the model library to the reconstruction, and the sum of the satisfied coefficients is equal to 1, ∑_{i=1}^N H_i = 1.

Taking the front 30° view angle of the car body as an example, 17 key points are selected with {Key P_i|i = 1, 2, 3, 4, 5, 12, 13, 14, 15, 16, 17, 18, 19, 22, 23, 24, 25} respective serials in every model are, {SK_j|j = 81, 85, 1, 5, 9, 45, 61, 64, 93, 113, 117, 124, 157, 104, 116, 172, 100} as shown in Fig.7.

The three coordinate values vector U_i for the specific 17 key points of every model S_i is calculated with U_i = (X_{SK81}ⁱ, Y_{SK81}ⁱ, Z_{SK81}ⁱ, X_{SK85}ⁱ, Y_{SK85}ⁱ, Z_{SK85}ⁱ, ..., X_{SK100}ⁱ, Y_{SK100}ⁱ, Z_{SK100}ⁱ)^T is a column matrix. Assume the rotation angle to the xyz coordinate system is [α, β, γ], according to the three-dimensional rotation matrix(equ.1), the rotation



FIGURE 7. 17 key points drawn in different car images.

relationship is as follows:

$$\begin{bmatrix} x' \\ y' \\ z' \end{bmatrix} = \begin{bmatrix} \cos\gamma & -\sin\gamma & 0 \\ \sin\gamma & \cos\gamma & 0 \\ 0 & 0 & 1 \end{bmatrix} \begin{bmatrix} \cos\beta & 0 & \sin\beta \\ 0 & 1 & 0 \\ -\sin\beta & 0 & \cos\beta \end{bmatrix} \times \begin{bmatrix} 1 & 0 & 0 \\ 0 & \cos\alpha & -\sin\alpha \\ 0 & \sin\alpha & \cos\alpha \end{bmatrix} \cdot \begin{bmatrix} x \\ y \\ z \end{bmatrix} \quad (1)$$

As there is only two-dimensional coordinate information, the yz plane projection of the 17 key points is carried out for every rotated model by equation 1 as U'_i , and the basement mat rix for the whole models of the 17 key points as $U' = [U'_1, U'_2, \dots, U'_{3528}]$, and define the y and z values of U' is K . The real 17 key points of the image can be obtained by labeling the image as Zt , the shape relation matrix is established

by them as $K \times H = Zt$. To solve the model contribution coefficient H , the optimization object is to minimize the cost function:

$$\min ||K_i H_i - Zt|| \quad (2)$$

constraining by

$$Zt = K_i \times H_i, \sum_{i=1}^N H_i = 1, 0 \leq H_i \leq 1 \quad (3)$$

Using the constrained least square method, the coefficient vector H can be obtained by. Further, the new model can be calculated according to formula (4).

$$newmodel = S \times H \quad (4)$$

And finally, the reconstruction 3D wire-frame model is shown in Fig.8.

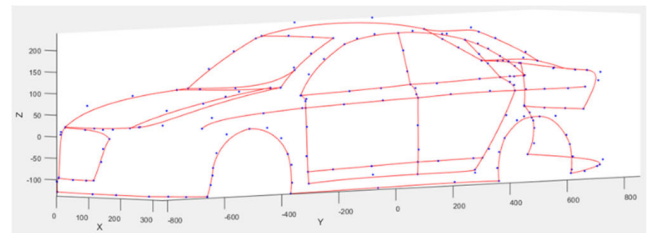


FIGURE 8. Reconstruct the 3D wireframe model.

Fig.9 shows the result of the Angle projection of the corresponding key points into the original image, where the red points are the manually selected key points, and the green points are the position points of the reconstructed projection. Red points are the original real position, and green ones are the reconstructed results.

Fig.10 is the reconstructed model corresponding to Fig.9 drawn in the image.

Similarly, select the key points of the rear 30° view Angle of the body and calculate the projection. 19key points are selected with $\{KeyP_i | i = 6, 7, 8, 9, 10, 11, 12, 13, 14, 15, 16, 17, 18, 19, 22, 23, 24, 25, 30\}$, respective serials in every model are $\{SK_j | j = 13, 17, 20, 25, 29, 37, 45, 61, 64, 93, 113, 117, 124, 157, 104, 108, 172, 100, 41\}$. Fig.11 shows the rendering result of the reconstructed model of the rear 30° view Angle of the body.

E. ERROR ANALYSIS

Since a single 2D image lacks depth information, there will be certain errors in reconstructing a 3D model based on 2D key point information. For side views and deflection views, the missing depth information is mainly in the x direction. In this paper, the key points manually extracted from the image are aligned with the key points of the model in the model library, and the missing depth information in the x direction is determined based on the best matching model.

The following is an analysis of model reconstruction errors for different brands of cars. The main contents include: 1) extracting key points from the reconstructed models of



FIGURE 9. Projection result for the front 30° view.

the front 30° view and the rear 30° view, and comparing them with the key points accurately extracted by the manual annotation method; 2) calculating the errors of all key points after reconstruction. The error analysis results are shown in Fig.12 and Fig.13.

From the error analysis results, it can be seen that the reconstruction error of the key points of the front 30° view is controlled within 60mm, and the reconstruction error of the key points of the rear 30° view is controlled within 55mm. Compared with the traditional reconstruction method, the reconstruction accuracy based on a single view is improved.

IV. SKELETON LINE EXTRACTION OF COMPLEX WIREFRAME MODEL

The modeling of complex body surfaces usually requires a lot of manpower operation, including the generation of NU-RBS spline curves and 3D body mesh. This paper relies on the 3D

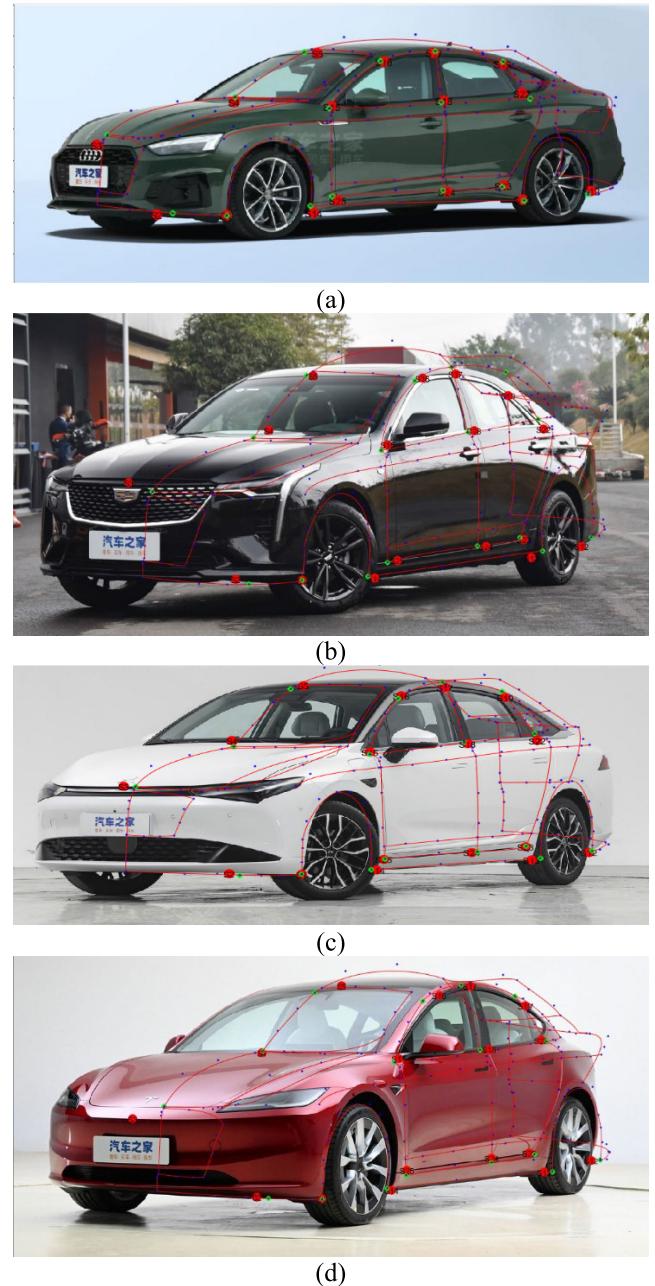


FIGURE 10. Fig. 7 corresponds to the drawing result of the reconstructed model in the image.

body contour model of cubic Bezier, splits the body surface into simple areas, and uses the square calculation of complex shape skeleton to get the best pair. Furthermore, the complex shape of the quadrilateral mesh generation, the final integration of the vehicle's three-dimensional quadrilateral control mesh results, and generate the body of the three-dimensional surface.

A. THE 3D WIRE-FRAME AREA OF THE BODY IS DIVIDED INTO BLOCKS

According to the characteristics of the body surface, the three-dimensional contour model of the entire body is divided

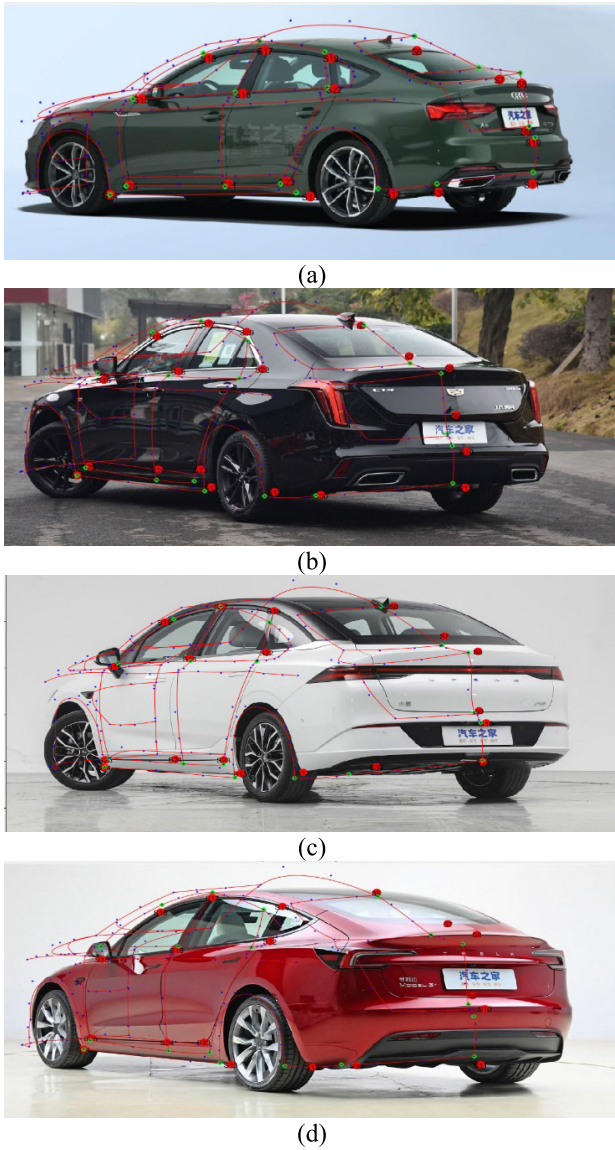


FIGURE 11. The reconstruction model drawing results in the rear 30° view of the car body.

into regions, as shown in Fig. 14 below, where different colors represent different regions, including 13 areas, such as the front face, engine hood, front window glass, top window glass, rear window glass, trunk cover, tail area, front wheel cover, side window, upper edge of side window, door, lower edge of door and rear wheel cover.

B. 2D PROJECTION OF COMPLEX SHAPES

To simplify the calculation, the corresponding relationship is generated on 2D complex shapes first. Take the complex shape of the wheel cover area as an example, project it onto the yz plane, generate boundary points with length 20 as the spacing, discretize the contour boundary of the wireframe in the clockwise direction and record the coordinate points, denoted as $P_i(i = 1, 2, \dots, n)$, corresponding to the normal direction PN_i . As shown in Fig. 15.

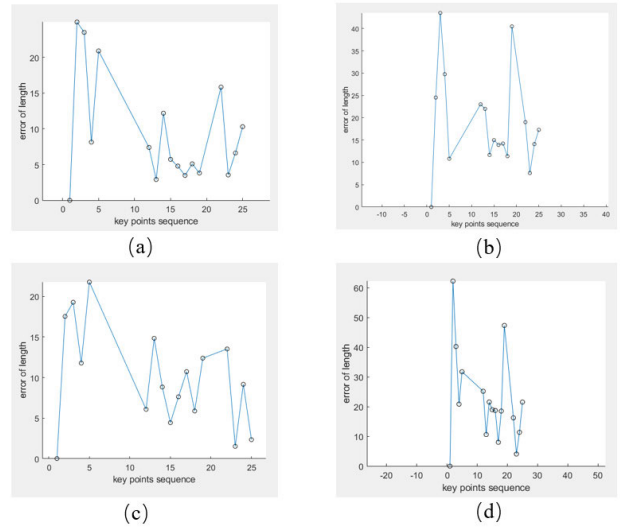


FIGURE 12. Key point reconstruction error of the front 30° view of the body.

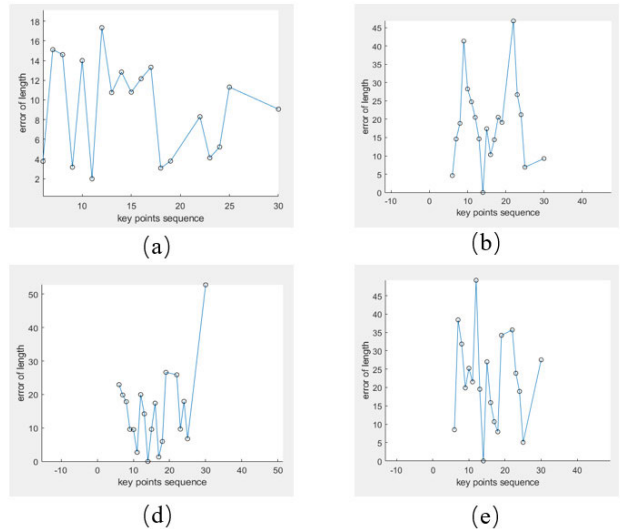


FIGURE 13. Key point reconstruction error in the rear 30° view of the body.

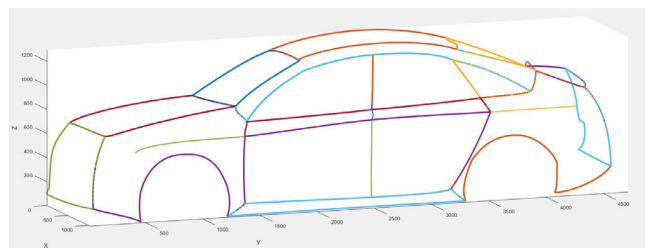


FIGURE 14. 3D block area.

C. OPTIMAL SKELETON WITH COMPLEX SHAPE

Taking skeleton lines as the midpoint of the optimal pair, this paper transforms the quadrilateral grid division problem of complex shapes into the extraction problem of the optimal skeleton lines. The following is an iterative method to

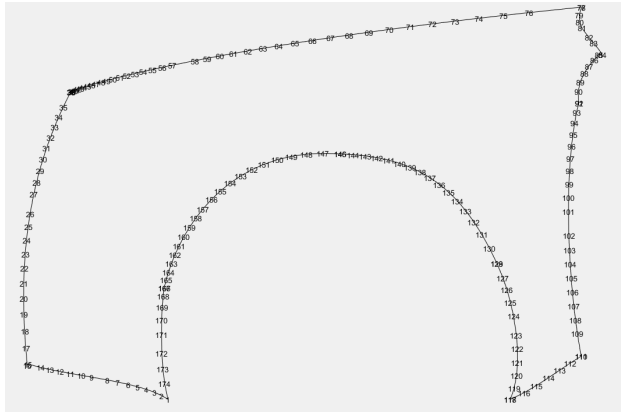


FIGURE 15. Complex shape projection.

calculate the optimal pair according to the area dichotomous relation.

First, taking a parallelogram as an example, the selection rule of its first optimal pair is shown in Fig.16, where the optimal pair corresponds to case 1. The specific steps are as follows:

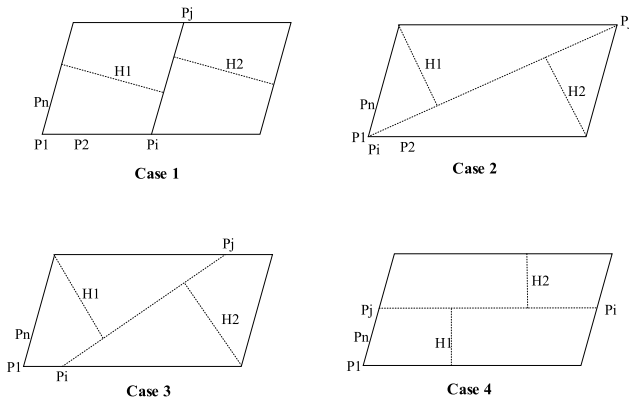


FIGURE 16. Optimal pair selection rule.

Take the area of the whole region as $allarea$ point to $P_i P_j$, the area of the left region is $area1$, the area of the right region is $area2$ and the maximum distance between the boundary point of the left region and $P_i P_j$ is $H1$ and the maximum distance between the boundary point of the right region and $P_i P_j$ is $H2$. The ratio of overlapping area to the whole area when the regions on both sides are folded as $P_i P_j$ is $arearatio$. The relation value $ijvalue$ is calculated according to formula (5). The selection rule of the optimal pair is $\max_{i,j}(ijvalue)$.

$$ijvalue = \frac{arearatio}{allarea} \times \frac{\min(area1, area2)}{\max(area1, area2)} \times \frac{\min(H1, H2)}{\max(H1, H2)} \times \frac{H1 + H2}{|P_i P_j|} \quad (5)$$

To speed up the calculation and optimize the point pair relationship, the following constraints are established in the

search for the most advantageous pair relationship:

$$\begin{aligned} \frac{|area1 + area2 - allarea|}{allarea} &< 0.1 \\ \frac{\max(area1, area2)}{\min(area1, area2)} &< 1.5 \\ \frac{\min(area1, area2)}{allarea} &> 0.3 \\ arearatio &> 0.2 \\ cos(PN_i, PN_j) &> 0.7 \end{aligned} \quad (6)$$

Among them, the above constraint condition (6) requires that the area difference of the two parts divided by $P_i P_j$ is as small as possible, the overlapping area is $arearatio > 0.2$, and the Angle between normal vectors should not be too large.

According to the iterative method, the optimal pair of regions is found successively, and finally, the optimal pair group of the whole region is established. The key steps of the algorithm include:

(1) Initialize $\{PI\}_i = \{P_i\}$, record all points of the serial number as $\{BI\}_i = [1, 2, \dots, n]$.

(2) The number of boundary points $\{PI\}_i$ is N_p , and the record $allarea = polyarea(\{PI\}_i)$; Calculate the overlap area-ratio of polygons on both sides $arearatio$; According to the discriminant condition 2, the optimal advantage pair relation is found, and the relation value $ijvalue$ of the point pair is calculated by the formula (5), and the optimal advantage pair is calculated and recorded as $[opt_i, opt_j]$. For each point pair, calculate the overlap area ratio $arearatio$. Check whether formula (5) is satisfied. If so, the optimal advantage pair is calculated and recorded as $[opt_i, opt_j]$.

(3) According to the optimal advantage pair relation obtained by the first calculation, the subsequent optimal advantage pair relation is calculated in sequence. Repeat until no new point pair relationships can be found.

(4) The skeleton line is composited by finding the two optimal midpoints from the original boundary points, and connecting these midpoints of boundary points in sequence to form a skeleton line.

(5) Output the sequence of optimal point pairs

The algorithm is as follows:

Fig.17 is the result of the point-pair relationship in the complex area of the front wheel cover shown in Fig.15.

The points composed of the midpoint sequence of the record point pair are listed as skeleton lines, where the first and last points are the midpoints on the original boundary, forming a complete path including the starting point, the middle point and the end point of the skeleton line. Finally, the path is drawn on the graph through the blue dashed line to visually show the skeleton line. Fig.18 shows the extraction results of skeleton lines(blue dashed line) with black lines as complex boundaries.

V. BODY SURFACE RECONSTRUCTION

According to the optimal sequence obtained by the algorithm, combined with the 3D control curve at the end of the skeleton

Algorithm 1 Skeleton Generation Algorithm for Complex Shape

Input: clockwise discrete wire frame boundary point $\{P_i\}$ and corresponding normal direction $\{PN_i\}$
Output: The most advantageous sequence number $\begin{bmatrix} KJ_1 \cdots KJ_k \cdots KJ_{k+1} \cdots KJ_N \\ KI_1 \cdots KI_k \cdots KI_{k+1} \cdots KI_N \end{bmatrix}$
 1: Initializ $\{PI_i\}=\{P_i\}$, record all points of the serial number as $\{BI_i\}=[1,2,\dots,n]$.
 2: Find optimal point pairs:
 Initialize $opti = 1, optj = 1$
 Iterate over all pairs (i, j) :
 Calculate areas $area1$ and $area2$
 Calculate overlap area ratio $arearatio$
 If $arearatio$ satisfies constraints (6)
 Calculate advantage value $ijvalue$
 If $ijvalue > optvalue$
 $Optvalue = ijvalue; opti = i; optj = j;$
 If no optimal pair is found, $opti=[]$, $optj=[]$;
 3: Iterate to calculate:
 Calculate the initial optimal pair $[opti0, optj0]$
 For $k = 1: N_{iter}$:
 Calculate optimal pair $[optik, optjk]$
 Repeat until no new pair is found
 4: Generate skeleton:
 Composite skeleton line by finding the optimal middle points and connecting them in boundary order
 5: Output the sequence of optimal point pairs

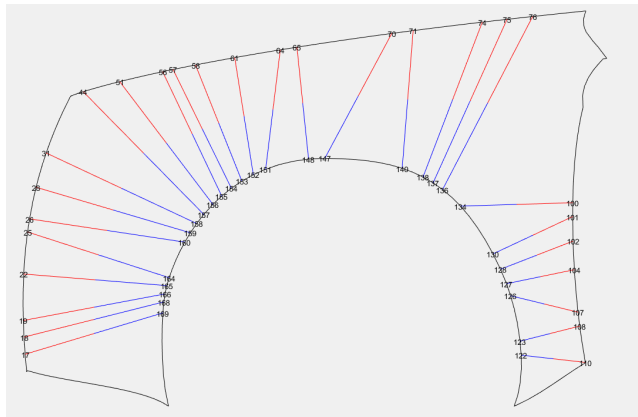


FIGURE 17. Boundary relation pair and curves at both ends.

line, the 3D control shape of the complex shape is restored. Finally, all areas are integrated to obtain the surface reconstruction results of the entire body.

Both ends of control curve $[BeginP0, BeginP1, BeginP2, BeginP3]$, $[EndP0, EndP1, EndP2, EndP3]$. It is rigidly scaled and rotated into $[[0,0],BP1, BP2,[1,0]]$ and $[[0,0],EP1, EP2,[1,0]]$ respectively, and then the three-dimensional control lines between the sequences are calculated according to the optimal sequence obtained by algorithm 1. The results are

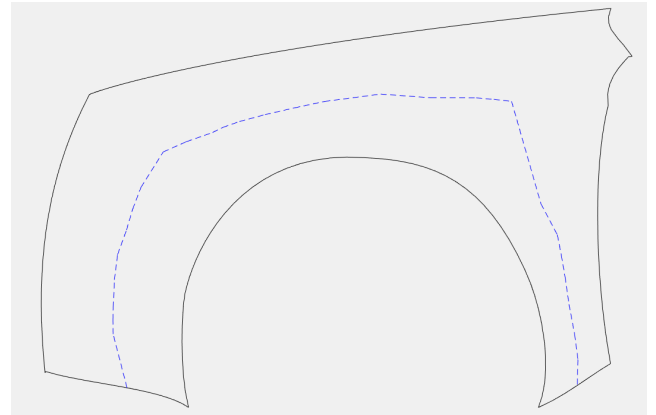


FIGURE 18. Extraction result of complex closed wire-frame skeleton.

as follows:

$$L_1^k = |P_0^2 - P_0^1| + \cdots + |P_0^{k+1} - P_0^k|$$

$$L_4^k = |P_3^2 - P_3^1| + \cdots + |P_3^N - P_3^{N-1}|$$

$$ratioP0_S = [L_1^1, \cdots, L_1^k, \cdots, L_1^{N-1}] / L_1^{N-1}$$

$$ratioP3_S = [L_4^1, \cdots, L_4^k, \cdots, L_4^{N-1}] / L_4^{N-1}$$

$$\{P_1^k\} = \times(1 - ratioP0_{S(k)})P_1^0 + \times ratioP0_{S(k)}P_1^{N+1}$$

$$\{P_2^k\} = \times(1 - ratioP0_{S(k)})P_2^0 + \times ratioP1_{S(k)}P_2^{N+1}$$

The combination of control points in the whole region is obtained as follows:

$$\begin{bmatrix} P_0^1 \cdots P_0^k \cdots P_0^{k+1} \cdots P_0^N \\ P_1^1 \cdots P_1^k \cdots P_1^k \cdots P_1^N \\ P_2^1 \cdots P_2^k \cdots P_2^{k+1} \cdots P_2^N \\ P_3^1 \cdots P_3^k \cdots P_3^k \cdots P_3^N \end{bmatrix}$$

The 3D rendering of the control polygon and the quadrilateral composed of the control polygon according to the obtained control points is shown in Fig.19.

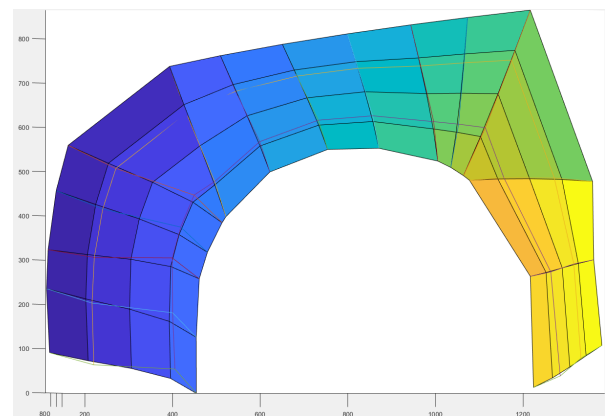


FIGURE 19. Control the generation of polygons.

As can be seen from the results in Fig.19, the corresponding relationship obtained at present is not detailed enough, and the corresponding relationship needs to be

further refined. The relational point pairs in the refining process are generated using the dynamic time adjustment (DTW) algorithm. According to the pair-to-pair distance between the point set $P(KI_k: KI_{k+1})$ and the point set $P(KJ_k: KJ_{k+1})$, the optimal correspondence relationship is found, and finally, a fine quadrilateral mesh is generated and 3D surfaces are drawn, as shown in Fig.20.

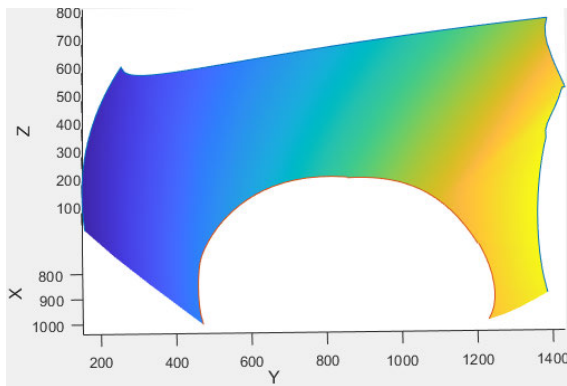


FIGURE 20. 3D surface generation.

By integrating all the body parts(Fig.21), the 3D surface result of the whole body can be obtained, as shown in Fig.22.

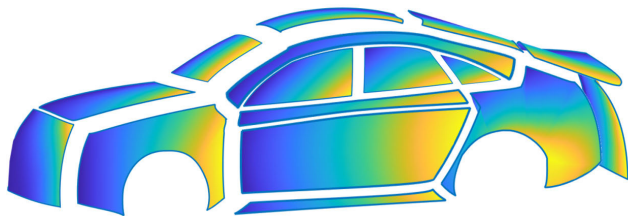


FIGURE 21. Surface result of every complex part.

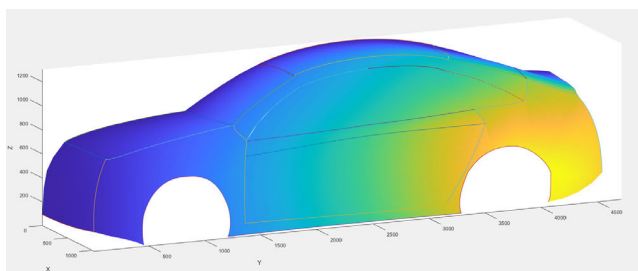


FIGURE 22. Integration of whole complex areas.

VI. CONCLUSION

In this paper, an automatic method of 3D wireframe and surface model reconstruction of a single car body image in any view is proposed. Firstly, a 3D wireframe model library was established to determine the key points of the car body. Based on the constructed MobileNet V2 vehicle view recognition system, the weight coefficients were calculated using the constrained least level method to complete the 3D wireframe model reconstruction under any view Angle. On this basis, the vehicle surface is divided into several blocks according

to the body parts, and the control polygon mesh of each block is generated by the skeleton line extraction algorithm to obtain the complex three-dimensional shape of the surface, and all the complex surfaces are integrated to achieve the three-dimensional surface reconstruction of the body.

In this paper, we take a sedan as an example to show in detail the complete process and effect of car body 3D surface reconstruction based on a single view. However, in practical applications, this method can be extended to other models. By establishing a database of different models, we can also use the method introduced in this paper to achieve car body 3D surface reconstruction.

The reconstruction accuracy of the car model is affected by the selection of key points and the number of model libraries. More appropriate key point selection and richer model libraries can significantly improve the accuracy of the reconstruction results. Therefore, future work can focus on the following two aspects:1) Analyze the styling features of different models and select key points to reduce reconstruction errors. By deeply studying the design features of different models, we can more accurately determine the key points, thereby improving the accuracy and quality of reconstruction. 2) Establish a larger number of model libraries to improve training accuracy. Expanding the scale of the model library will provide the algorithm with more diverse training data, thereby enhancing its generalization ability and accuracy. By carrying out further work on the above two aspects, we can continuously improve the level of car body 3D surface reconstruction technology to better meet the needs of practical applications.

REFERENCES

- [1] Z. Wang, Y. Zhong, S.-L. Chai, S.-F. Niu, M.-L. Yang, and G.-R. Wu, "Product design evaluation based on improved CRITIC and comprehensive cloud-TOPSIS—Applied to automotive styling design evaluation," *Adv. Eng. Informat.*, vol. 60, Apr. 2024, Art. no. 102361.
- [2] T. J. S. Anand, H. H. H. Afandi, I. S. Othman, S. I. A. Razak, and R. S. S. Singh, "Static analysis for nickel aluminides (Ni_3Al) wheel hub using CATIA and solidworks," *Aeronaut. Aerosp. Open Access J.*, vol. 6, no. 5, pp. 166–169, Oct. 2022.
- [3] A. Arora, A. Pathak, A. Juneja, P. Shakkurwal, and R. Kumar, "Design & analysis of progressive die using solid works," *Mater. Today, Proc.*, vol. 51, pp. 956–960, Jun. 2022.
- [4] Z. Tao, Q. Xu, X. Liu, and J. Liu, "An integrated approach implementing sliding window and DTW distance for time series forecasting tasks," *Int. J. Speech Technol.*, vol. 53, no. 17, pp. 20614–20625, Sep. 2023.
- [5] H.-Y. Lin, C.-L. Tsai, and V. L. Tran, "Depth measurement based on stereo vision with integrated camera rotation," *IEEE Trans. Instrum. Meas.*, vol. 70, pp. 1–10, 2021.
- [6] X. Song, G. Yang, X. Zhu, H. Zhou, Z. Wang, and J. Shi, "AdaStereo: A simple and efficient approach for adaptive stereo matching," in *Proc. IEEE/CVF Conf. Comput. Vis. Pattern Recognit. (CVPR)*, Jun. 2021, pp. 10323–10332.
- [7] L. Melas-Kyriazi, C. Rupprecht, and A. Vedaldi, "PC2: Projection-conditioned point cloud diffusion for single-image 3D reconstruction," in *Proc. IEEE/CVF Conf. Comput. Vis. Pattern Recognit. (CVPR)*, Jun. 2023, pp. 12923–12932.
- [8] F. Zhang, W. Zhang, Q. Lei, X. Li, Y. Li, and M. Xu, "Voxel-free neural volume reconstruction technique for volumetric flame reconstructions," *Aerosp. Sci. Technol.*, vol. 133, Feb. 2023, Art. no. 108107.
- [9] J. Liu, P. Ji, N. Bansal, C. Cai, Q. Yan, X. Huang, and Y. Xu, "PlaneMVS: 3D plane reconstruction from multi-view stereo," in *Proc. IEEE/CVF Conf. Comput. Vis. Pattern Recognit. (CVPR)*, Jun. 2022, pp. 8655–8665.

- [10] J. Liu, J. Gao, S. Ji, C. Zeng, S. Zhang, and J. Gong, "Deep learning based multi-view stereo matching and 3D scene reconstruction from oblique aerial images," *ISPRS J. Photogramm. Remote Sens.*, vol. 204, pp. 42–60, Oct. 2023.
- [11] H. Chen and Y. Zuo, "3D-ARNet: An accurate 3D point cloud reconstruction network from a single-image," *Multimedia Tools Appl.*, vol. 81, no. 9, pp. 12127–12140, Sep. 2021.
- [12] J. Hou, L. Yu, and S. Fei, "A high-quality voxel 3D reconstruction system for large scenes based on the branch and bound method," *Expert Syst. Appl.*, vol. 194, May 2022, Art. no. 116549.
- [13] W. Burger and M. J. Burge, "Scale-invariant feature transform (SIFT)," *Digital Image Proc. Alg. Intro.*, pp. 709–763, Jul. 2022.
- [14] G. Fahim, K. Amin, and S. Zarif, "Single-view 3D reconstruction: A survey of deep learning methods," *Comput. Graph.*, vol. 94, pp. 164–190, Feb. 2021.
- [15] J. Han, Y. Cao, L. Xu, W. Liang, Q. Bo, J. Wang, C. Wang, Q. Kou, Z. Liu, and D. Cheng, "3D reconstruction method based on medical image feature point matching," *Comput. Math. Methods Med.*, vol. 2022, pp. 1–11, Aug. 2022.
- [16] F. Engelmann, K. Rematas, B. Leibe, and V. Ferrari, "From points to multi-object 3D reconstruction," in *Proc. IEEE/CVF Conf. Comput. Vis. Pattern Recognit. (CVPR)*, Jun. 2021, pp. 4586–4595.
- [17] K. Fu, J. Peng, Q. He, and H. Zhang, "Single image 3D object reconstruction based on deep learning: A review," *Multimedia Tools Appl.*, vol. 80, no. 1, pp. 463–498, Jan. 2021.
- [18] W. Chen, G. Shang, A. Ji, C. Zhou, X. Wang, C. Xu, Z. Li, and K. Hu, "An overview on visual SLAM: From tradition to semantic," *Remote Sens.*, vol. 14, no. 13, p. 3010, Jun. 2022.
- [19] S. Wang, Z. Tian, K. Dong, and Q. Xie, "Inconsistency of neighborhood based on Voronoi tessellation and Euclidean distance," *J. Alloys Compounds*, vol. 854, Feb. 2021, Art. no. 156983.
- [20] M. H. Qais, H. M. Hasanien, R. A. Turkey, S. Alghuwainem, M. Tostado-Véliz, and F. Jurado, "Circle search algorithm: A geometry-based metaheuristic optimization algorithm," *Mathematics*, vol. 10, no. 10, p. 1626, May 2022.
- [21] H. Duan, Y. Zhao, K. Chen, D. Lin, and B. Dai, "Revisiting skeleton-based action recognition," in *Proc. IEEE/CVF Conf. Comput. Vis. Pattern Recognit. (CVPR)*, Jun. 2022, pp. 2959–2968.
- [22] L. Dang, Y. Nie, C. Long, Q. Zhang, and G. Li, "MSR-GCN: Multi-scale residual graph convolution networks for human motion prediction," in *Proc. IEEE/CVF Int. Conf. Comput. Vis. (ICCV)*, Oct. 2021, pp. 11447–11456.
- [23] K. Hu, Y. Ding, J. Jin, L. Weng, and M. Xia, "Skeleton motion recognition based on multi-scale deep spatio-temporal features," *Appl. Sci.*, vol. 12, no. 3, p. 1028, Jan. 2022.
- [24] Z. Huang, Y. Wen, Z. Wang, J. Ren, and K. Jia, "Surface reconstruction from point clouds: A survey and a benchmark," 2022, *arXiv:2205.02413*.
- [25] T. Wu, J. Wang, X. Pan, X. Xu, C. Theobalt, Z. Liu, and D. Lin, "Voxurf: Voxel-based efficient and accurate neural surface reconstruction," 2022, *arXiv:2208.12697*.
- [26] C. Lv, W. Lin, and B. Zhao, "Voxel structure-based mesh reconstruction from a 3D point cloud," *IEEE Trans. Multimedia*, vol. 24, pp. 1815–1829, 2022.
- [27] B. Ummenhofer and V. Koltun, "Adaptive surface reconstruction with multiscale convolutional kernels," in *Proc. IEEE/CVF Int. Conf. Comput. Vis. (ICCV)*, Oct. 2021, pp. 5631–5640.
- [28] A. Perney, S. Bordas, and P. Kerfriden, "NURBS-based surface generation from 3D images: Spectral construction and data-driven model selection," *J. Comput. Des. Eng.*, vol. 10, no. 4, pp. 1856–1867, Jul. 2023.
- [29] S. S. Raseli, N. A. M. K. Faisal, and N. Mahat, "The construction of cubic Bezier curve," *J. Comput. Res. Innov.*, vol. 7, no. 2, pp. 111–120, Sep. 2011.
- [30] S. Ashwinkumar, S. Rajagopal, V. Manimaran, and B. Jegajothi, "Automated plant leaf disease detection and classification using optimal MobileNet based convolutional neural networks," *Mater. Today, Proc.*, vol. 51, no. 1, pp. 480–487, Feb. 2022.
- [31] P. N. Srinivasu, J. G. Sivasai, M. F. Ijaz, A. K. Bhoi, W. Kim, and J. J. Kang, "Classification of skin disease using deep learning neural networks with MobileNet V2 and LSTM," *Sensors*, vol. 21, no. 8, p. 2852, Apr. 2021.
- [32] M. Iman, H. R. Arabnia, and K. Rasheed, "A review of deep transfer learning and recent advancements," *Technologies*, vol. 11, no. 2, p. 40, Mar. 2023.
- [33] M. Yuan, X. Bi, X. Huang, W. Zhang, L. Hu, G. Y. Yuan, and Y. Sun, "Towards time-series key points detection through self-supervised learning and probability compensation," in *Proc. IEEE Int. Conf. Database Syst. Adv. Appl., Ari.*, 2023, pp. 237–252.



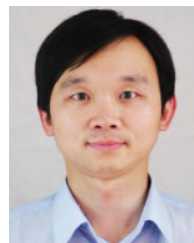
BO WANG received the Ph.D. degree from Dalian University of Technology, Liaoning, in 2017. She is currently a Lecturer with Wuhan University of Science and Technology, Wuhan, China, where she mainly teaches and researches in vehicle engineering. She has chaired two National Natural Science Foundation projects. Her main research interest includes body CAD/CAS.



QI WU received the bachelor's degree in vehicle engineering from Wuhan Business University, Wuhan, China, in 2019. He is currently pursuing the master's degree in vehicle engineering with Wuhan University of Science and Technology. His current research interest includes body CAD/CAS.



HUAWEI WANG received the Ph.D. degree from Huazhong University of Science and Technology, in 2019. He is currently a Lecturer with Wuhan University of Science and Technology, Wuhan, China. He is mainly engaged in teaching and research in vehicle engineering. His research interests include electro-hydraulic hybrid drives, energy conservation, and vibration and noise reduction.



LI HU received the Ph.D. degree from Huazhong University of Science and Technology, in 2008. He is currently a Professor with Wuhan University of Science and Technology, Wuhan, China. He is mainly engaged in vehicle engineering teaching and research. His main research interests include noise and vibration control, automotive NVH, and sound quality.



BAOJUN LI (Member, IEEE) received the Ph.D. degree from Dalian University of Technology, Dalian, Liaoning, in 2009. He is currently an Associate Professor with Dalian University of Technology. He presided over and participated in more than 20 national, provincial, and ministerial research projects, including two 973 subprojects, two 863 subprojects, and seven National Natural Science Foundation projects. He has published more than 70 academic papers in high-level academic journals and academic conferences, applied for and obtained more than ten national invention patents and appearance patents, and 12 software copyrights. His research interests include big data-driven product intelligent design and integrated design, robotics and autonomous driving technology, and deep learning. He won the Second Prize in Liaoning Province Natural Science Academic Achievement Award for two consecutive years, in 2011 and 2012.

...